THE JOURNAL OF BIOLOGICAL CHEMISTRY VOL. 290, NO. 28, pp. 17401–17414, July 10, 2015

Generation of Dopamine Neurons from Rodent Fibroblasts through the Expandable Neural Precursor Cell Stage*

Received for publication, December 2, 2014, and in revised form, May 5, 2015 Published, JBC Papers in Press, May 28, 2015, DOI 10.1074/jbc.M114.629808

Mi-Sun Lim[‡§¶1], Mi-Yoon Chang[§‖1], Sang-Mi Kim[**], Sang-Hoon Yi[§‖], Haeyoung Suh-Kim[‡‡], Sung Jun Jung[§ §§], Min Jung Kim[§ §§], Jin Hyuk Kim[‡§ §§], Yong-Sung Lee[‡§‖], Soo Young Lee[¶], Dong-Wook Kim[¶¶], Sang-Hun Lee[§‖2], and Chang-Hwan Park[‡§¶3]

From the [‡]Graduate School of Biomedical Science and Engineering, the [§]Hanyang Biomedical Research Institute, the [**]Department of Biomedical Science, Graduate School, and the Departments of [¶]Microbiology, [§§]Physiology, and [‖]Biochemistry and Molecular Biology, College of Medicine, Hanyang University, Seoul 133-791, Korea, the [‡‡]Department of Anatomy and Brain Disease Research Center, College of Medicine, Ajou University, Suwon 443-749, Korea, and the [¶¶]Department of Physiology and Cell Therapy Center, Yonsei University College of Medicine, Seoul 120-752, Korea

Background: Fibroblasts can be converted into neurons by transduction with BAM.
Results: Multiple lines of evidence were used to demonstrate that a significant percentage of BAM-transduced fibroblasts can be converted into iNPCs by co-expression of *Bcl-xL*.
Conclusion: BAMX-derived iNPCs were expandable over multiple passages *in vitro*, and differentiation phenotypes of iNPCs were readily manipulated by specific developmental cues.
Significance: *Bcl-xL* has a critical role in neural precursor cell conversion.

Recent groundbreaking work has demonstrated that combined expression of the transcription factors *Brn2*, *Ascl1*, and *Myt1L* (BAM; also known as Wernig factors) convert mouse fibroblasts into postmitotic neuronal cells. However, questions remain regarding whether trans-conversion is achieved directly or involves an intermediary precursor stage. Trans-conversion toward expandable neural precursor cells (NPCs) is more useful than direct one-step neuron formation with respect to yielding a sufficient number of cells and the feasibility of manipulating NPC differentiation toward certain neuron subtypes. Here, we show that co-expression of Wernig factors and *Bcl-xL* induces fibroblast conversion into NPCs (induced NPCs (iNPCs)) that are highly expandable for >100 passages. Gene expression analyses showed that the iNPCs exhibited high expression of common NPC genes but not genes specific to defined embryonic brain regions. This finding indicated that a regional identity of iNPCs was not established. Upon induction, iNPCs predominantly differentiated into astrocytes. However, the differentiation potential was not fixed and could be efficiently manipulated into general or specific subtypes of neurons by expression of additional genes. Specifically, overexpression of *Nurr1* and *Foxa2*, transcription factors specific for midbrain dopamine neuron development, drove iNPCs to yield mature midbrain dopamine neurons equipped with presynaptic DA neuronal functions. We further assessed the therapeutic potential of iNPCs in Parkinson disease model rats.

Somatic cell reprogramming has long been an active area of stem cell research. After developing approaches for dedifferentiation of somatic cells into Embryonic stem-like pluripotent cells using somatic cell nuclear transfer (1, 2) and cell fusion (3, 4), Takahashi and Yamanaka (5) demonstrated that forced expression of a set of reprogramming factors converts fibroblasts to a pluripotent state, after which they become induced pluripotent stem cells (iPSCs).[4] Techniques involving iPSCs have opened several new avenues for disease modeling and personalized cell replacement therapies. However, the potential for tumor formation by undifferentiated cells and/or the exogenous introduction of reprogramming factors remains a critical concern with respect to iPSC-based therapeutic approaches.

Direct conversion from a somatic cell type into another tissue-specific cell without passing through a pluripotent state may circumvent the safety issues associated with using iPSCs. Wernig and colleagues (6) provided the first evidence of such a direct conversion, in which expression of a combination of neuronal lineage-inducing transcription factors (*Brn2*, *Ascl1*, and *Myt1L* (BAM); also known as Wernig factors) efficiently con-

* This work was supported by Medical Research Center Grant 2008-0062190; Basic Science Research Program Grant 2011-0008952; Bio & Medical Technology Development Program Grants 2010-0020232 and 2012 M3A9C7050126; and Korea National Research Council of Science and Technology Program Grant NAP-09-04 through the National Research Foundation of Korea (NRF) funded by the Ministry of Science, ICT, and Future Planning.

[1] Both authors contributed equally to this work.

[2] To whom correspondence may be addressed: Dept. of Biochemistry and Molecular Biology, College of Medicine, Hanyang University, 222 Wangsimni-ro, Seongdong-gu, Seoul, 133-791, Korea; Tel.: 82-2-2220-0625; Fax: 82-2-2220-2422; E-mail: leesh@hanyang.ac.kr.

[3] To whom correspondence may be addressed: Laboratory of Neural Stem Cell Biology, Graduate School of Biomedical Science and Engineering and Dept. of Microbiology, College of Medicine, Hanyang University, 222 Wangsimni-ro, Seongdong-gu, Seoul 133-791, Korea. Tel.: 82-2-2220-0646; Fax: 82-2-2220-2422; E-mail: chshpark@hanyang.ac.kr.

[4] The abbreviations used are: iPSC, induced pluripotent stem cell; NPC, neural precursor cell; iNPC, induced NPC; REF, rat embryonic fibroblast; MEF, mouse embryonic fibroblast; NIM, neural induction medium; TH, tyrosine hydroxylase; DA, dopamine; mDA, midbrain-type DA; Parkinson disease; TTF, tail tip fibroblast; bFGF, basic fibroblast growth factor; LIF, leukemia inhibitory factor; DAB, 3,3′-diaminobenzidine; SMA, smooth muscle actin; GFAP, glia fibrillary acidic protein; BAM, *Brn2*, *Ascl1*, and *Myt1L*; BAMX, BAM + *Bcl-xL*; N+F, *Nurr1* and *Foxa2*.

verted mesodermal mouse fibroblasts into induced neuronal cells.

Direct conversion is a conceptually interesting process but is not very practical for research or therapy because direct 1:1 conversion can yield only a limited number of trans-converted cells. Furthermore, terminally differentiated cells are expected to integrate into and survive in host tissues poorly after transplantation compared with proliferating somatic precursor cells. Thus, conversion into expandable precursors is considered a better approach. Indeed, in the last several years, multiple protocols for the conversion of fibroblasts into neural precursor cells (NPCs) with self-renewal capacity have been developed using forced expression of diverse gene combinations (7–11).

Considering that somatic cells are generated sequentially via their intermediary tissue-specific precursors during *in vivo* development, direct trans-differentiation into another type of terminally differentiated cells is probably irrelevant from a physiological standpoint. Thus, an interesting but unanswered question is whether somatic cell conversions are induced under artificial conditions without passing through intermediate somatic precursor cell stages. To address this question, we utilized Wernig factor-based fibroblast-to-neuron conversion. Specifically, we utilized multiple lines of evidence to clearly demonstrate that a significant portion of BAM-transduced fibroblasts, if not all, can be converted into NPCs (referred as to induced NPCs (iNPCs)) by co-expression of BAM with *Bcl-xL*. Importantly, iNPCs exhibited a high capacity for self-renewal over a long period in culture as well as a propensity for easily manipulated differentiation. We further assessed the therapeutic potential of iNPCs in a Parkinson disease (PD) rat model.

Materials and Methods

Fibroblast Isolation—Animals were housed and treated according to the institutional animal care and use committee guidelines of Hanyang University. Fibroblasts from CF1 mice (Charles River Laboratories, Wilmington, MA), ICR mice, C57/BL6 mice (DaeHan BioLink, Seoul, Korea), and pNestin-GFP mice were isolated from embryonic day 13.5 embryos (MEFs). Fibroblasts from Sprague-Dawley (DaeHan BioLink), Lewis, and Wistar rats (Central Lab. Animal Inc., Seoul, Korea) were isolated from embryos after removing the head, spinal cord, and all internal organs, including the gonads (REFs). Adult tail tip fibroblasts (TTFs) were kindly provided by Jeong Tae Do (Konkuk University, Seoul, Korea). Fibroblasts were cultured in Dulbecco's modified Eagle's medium (DMEM) with high glucose (Invitrogen) containing 10% fetal bovine serum (FBS; Invitrogen), 0.1 mM nonessential amino acids (Invitrogen), 0.1 mM β-mercaptoethanol (Sigma-Aldrich), 2 mM L-glutamine (Sigma-Aldrich), and 1% penicillin-streptomycin (Invitrogen).

Retroviral Production—Retroviral constructs for *Brn2*, *Ascl1*, *Myt1L*, *Bcl-xL*, *Bcl-xL*-Y101K, *Bcl-xL*-R209X (12), CA-*Akt*, CA-*Raf*, *Wnt1*, *Dlx2*, *Otx2*, *Nurr1*, *Foxa2*, and *Ngn2* were constructed by engineering the appropriate DNA fragments into the pCL retroviral vector (13). Retroviral vectors were transfected into 293GPG packaging cells using Lipofectamine 2000 reagent (Invitrogen). Supernatants containing viral particles were harvested 72 h after transfection.

iNPC Generation and Isolation—For generation of iNPCs, fibroblasts were seeded on gelatin-coated culture dishes (0.5–1×10^6 cells/100-cm dish). The next day, the cells were transduced with three retroviruses for BAM and additional factors as indicated. After 16–20 h, the culture medium was changed to fresh fibroblast medium containing 100 ng/ml human fibroblast growth factor 8 (FGF8; Peprotech, Rocky Hill, NJ).

After 2 days, transduced cells were placed in neural induction medium (NIM; N2 medium supplemented with 20 ng/ml basic fibroblast growth factor (bFGF; R&D Systems, Minneapolis, MN), 100 ng/ml FGF8, 100 units/ml recombinant human leukemia inhibitory factor (LIF; Millipore, Billerica, MA), and 2 μg/ml doxycycline (Dx; Sigma-Aldrich)), and the culture medium was changed every other day thereafter. Two days after initiating NIM culture conditions, cells were transferred to 6-well culture dishes precoated with 15 μg/ml poly-L-ornithine (Sigma-Aldrich) and 1 μg/ml of fibronectin (Sigma-Aldrich) and maintained in NIM. After ~2–3 weeks, the cell morphology changed to that of neural stem-like cells as evidenced by a small cell size and bipolar morphology. Formation of cell clusters was also observed.

Induced Dopamine Neuron Generation from Fibroblast-derived iNPCs—For generation of dopaminergic neurons, iNPCs were transferred onto coverslips (Bellco Glass, Vineland, NJ) precoated with poly-L-ornithine/fibronectin. After 1 day, iNPCs were transduced for 2 h with the dopaminergic neuron-related factors *Nurr1* and *Foxa2* as well as *Ngn2* for mouse cells and were then cultured overnight in NIM and differentiated the following day in medium containing 0.2 mM ascorbic acid (Sigma-Aldrich), 20 ng/ml brain-derived neurotrophic factor (R&D Systems), 20 ng/ml glial cell line-derived neurotrophic factor (R&D Systems), and 250 μg/ml dibutyryl-cAMP (Sigma-Aldrich) in N2 medium.

Reverse Transcription-Polymerase Chain Reaction (RT-PCR) and Real-time PCR—Total cellular RNA was isolated using TRI REAGENT (Molecular Research Center, Inc., Cincinnati, OH), and cDNA was synthesized from 5 μg of total RNA in a 20-μl reaction volume using the Superscript kit (Invitrogen). The PCR conditions are provided in Table 1. Real-time PCR analyses were performed as described previously (14). Real-time PCR was performed on a CFX96 real-time system using iQ SYBR Green supermix (Bio-Rad). The PCR conditions are summarized in Table 2.

Immunostaining of Cultured Cells and Brain Tissues—Immunostaining of cultured cells and brain tissues was performed as described previously (14). Cells were photographed using epifluorescence and a confocal microscope (Leica Microsystems, Wetzlar, Germany). Measurement of tyrosine hydroxylase (TH) fiber length was computed with the Leica Application Suite image analysis package. Primary antibody information is summarized in Table 3.

Electrophysiology—Whole-cell patch recordings were performed at 22 ± 1 °C with an EPC10 USB amplifier (HEKA Elektronik, Lambrecht, Germany). The bath solution consisted of 124 mM NaCl, 26 mM $NaHCO_3$, 3.2 mM KCl, 2.5 mM $CaCl_2$, 1.3 mM $MgCl_2$, 1.25 mM $NaHPO_4$, and 10 mM glucose

TABLE 1
Gene-specific primer sequences and RT-PCR conditions

Gene	PCR sequence (5′–3′)	Annealing temperature	Cycle	Product size
		°C		*bp*
Th				
Forward	TCAAGACTGACTCACAGCAACCCC	60	25	412
Reverse	CTTTGTCCTGAACCGTGGTGGTAG			
Gapdh				
Forward	GGCATTGCTCTCATTGACAA	60	23	165
Reverse	AGGGCCTCTCTCTTGCTCTC			

TABLE 2
Gene-specific primer sequences for real-time PCR
Real-time PCR conditions were as follows: 60 °C annealing temperature and 40 cycles.

Gene	Forward sequence	Reverse sequence
Nestin	CTGAGGCCTCTCTTCTTCCA	ACCCTGTACCGGGTCTCCT
Sox2	CCCCCGGCGGCAATAGCA	TGGGCGAGCCGTTCATGTAGGTCT
Pax6	CCAAAGTGGTGGACAAGATTGCC	TAACTCCGCCCATTCACTGACG
Bf1 (*FoxG1*)	TCGTAAAACTTGGCAAAGAGGG	GCTGTTCGCAAAGACTCGCTAC
Emx2	TTCGAACCGCCTTCTCGCCG	TGAGCCTTCTTCCTCTAG
Pax5	ATGCAACTGATGGAGTATGAGGAGCC	CAGATGTAGTCCGCCAAAGGATAG
En1/2	TCAAGACTGACTCACAGCAACCCC	CTTTGTCCTGAACCGTGGTGGTAG
Otx2	CCATGACCTATACTCAGGCTTCAGG	GAAGCTCCATATCCCTGGGTGGAAAG
Lmx1a	CCCCAAAATCCGGAATTACT	CTCAGGGTCAGCAAAAGGAG
Foxa2	GCTCCCTACGCCAATATCAA	CCGGTAGAAAGGGAAGAAGT
Nkx6.1	TCAGGTCAAGGTCTGGTTCC	CCAGGGGCTTGTTGTAATCG
Nkx6.2	TCTCTGGCCAGCAGATCTTC	TACTCGTCATCATCCTCCGC
HoxB1	TACAAACTTCACCACACGCC	GCTCGCGTTTCTTTTGCTTC
HoxB4	GTAAACCCCAATTACGCCGG	CGCCGATTTTGGAACCAGAT
HoxC8	ATCCTCCGCCAACACTAACA	CGGCGCTTTCTGGTCAAATA
Gbx2	GGCAACTTCGACAAATCCGA	CTGGCCAGGCAAATTGTCAT
Gapdh	GGCATTGCTCTCATTGACAA	AGGGCCTCTCTCTTGCTCTC

TABLE 3
Primary antibody information

Antibody	Dilution	Source	Location
Polyclonal antibody (rabbit)			
Nestin #130 (NES)	1:50	Dr. R. McKay (NIH)	Bethesda, MD
Tyrosine hydroxylase (TH)	1:5000	Pel-Freez	Rogers, AR
GABA	1:5000	Sigma-Aldrich	St. Louis, MO
Neuron-specific class III β-tubulin (TUJ1)	1:5000	Covance	Richmond, CA
Glia fibrillary acidic protein (GFAP)	1:400	DAKO	Glostrup, Denmark
Potassium inwardly rectifying channel subfamily J, member 6 (GIRK2)	1:100	Sigma-Aldrich	St. Louis, MO
Green fluorescent protein (GFP)	1:2000	Life Technologies	Eugene, OR
SOX2	1:500	Chemicon	Temecula, CA
PITX3	1:200	Chemicon	Temecula, CA
Vesicular monoamine transporter 2 (VMAT2)	1:500	Pel-Freez	Rogers, AR
NURR1	1:500	Santa Cruz Biotechnology	Dallas, TX
Synapsin I	1:1000	Sigma-Aldrich	St. Louis, MO
Collagen I	1:500	Abcam	Cambridge, UK
Cleaved caspase-3	1:500	Cell Signaling	Danvers, MA
Serotonin	1:4000	Sigma-Aldrich	St. Louis, MO
Monoclonal antibody (mouse)			
Nestin (NES)	1:500	BD Biosciences	Franklin Lakes, NJ
TH	1:2000	Sigma-Aldrich	St. Louis, MO
TUJ1	1:2000	Covance	Richmond, CA
CNPase	1:500	Sigma-Aldrich	St. Louis, MO
Microtubule-associated protein 2 (MAP2)	1:1000	Sigma-Aldrich	St. Louis, MO
GFAP	1:500	MP Biomedicals	Santa Ana, CA
Glutamate clone glu4 (GluT)	1:5000	Sigma-Aldrich	St. Louis, MO
Smooth muscle actin (SMA)	1:1000	Sigma-Aldrich	St. Louis, MO
KI67	1:100	Novocastra	Newcastle, UK
HuC/D	1:100	Chemicon	Temecula, CA
Other host			
Dopamine transporter (DAT), anti-rat	1:200	Abcam	Cambridge, UK
FOXA2, anti-goat	1:500	Santa Cruz Biotechnology	Dallas, TX

saturated with 95% O_2 and 5% CO_2. The pipette (3–4-megaohm) solution for whole-cell patch clamp recordings consisted of 140 mM potassium gluconate, 5 mM di-Tris-phosphocreatine, 5 mM NaCl, 4 mM MgATP, 0.4 mM Na_2GTP, 15 mM HEPES, and 2.5 mM sodium pyruvate at pH 7.3 (adjusted with KOH).

Fluorescence-activated Cell Sorting (FACS) and Cell Cycle Analysis—pNestin-GFP MEF-derived iNPCs were analyzed and sorted using a FACSCalibur flow cytometer (BD Biosciences, Franklin Lakes, NJ). Data were analyzed using CellQuest Pro software (BD Biosciences). For cell cycle analysis, BAMX-transduced iNPCs derived from MEFs or REFs were

resuspended in 50 μg/ml propidium iodide (Invitrogen) and 250 μg/ml RNase A (Thermo Fisher Scientific). A FACSCanto II (BD Biosciences) was used for analysis, and cytometer readings were evaluated using the 488-nm emission filter.

In Vivo Transplantation and Histological Procedures—*In vivo* transplantation and histological procedures were performed as described previously (14). iNPCs were deposited at two sites (coordinates in anterior/posterior, medial/lateral, and dorsal/ventral relative to the bregma and dura: 1) +0.07, −0.30, −0.55; 2) −0.1, −0.40, −0.50; incisor bar set at 3.5 mm below 0) while the animal was under anesthesia induced by Zoletil 50 (3.3 mg/kg; Virbac Laboratories, Carros, France) mixed with Rompun (93.3 μg/kg; Bayer Korea, Seoul, Korea). The needle was left in place for 5 min following each injection. Amphetamine-induced rotations were determined 2, 4, 6, 8, and 10 weeks after transplantation.

Three and 8 weeks after transplantation, animals were anesthetized and perfused intracardially with 4% paraformaldehyde. To compensate for double counting in adjacent sections, we used the Abercrombie correction factor ($N = n \times T/(T + D)$, where N is the actual number of cells, n is the number of nuclear profiles, T is the section thickness, and D is the average diameter of nuclei). Graft areas were determined using Leica Application Suite image analysis, and the Cavalieri estimator was used to calculate graft volumes.

3,3′-Diaminobenzidine (DAB) Staining—Free-floating 30-μm sections were collected and processed for immunohistochemistry using DAB staining. Sections were washed in 0.1% BSA/PBS and then incubated in 0.3% hydrogen peroxide for 1 h at room temperature. The sections were blocked with 10% normal goat serum and 0.3% Triton X-100 in 0.1% BSA/PBS for 1 h and incubated overnight with primary antibody (TH 1:250; Pel-Freez) at 4 °C in 0.1% BSA/PBS containing 10% normal goat serum. After rinsing, sections were incubated with a biotinylated antibody (1:250; Vector Laboratories) for 1 h.

After washing, the sections were incubated in horseradish peroxidase streptavidin (1:400; Vector Laboratories) for 2 h. The sections were then washed and visualized using DAB tetrahydrochloride (SK-4100; Vector Laboratories) for 10–30 s. Development was quenched with distilled water, and each section was mounted on a slide, air-dried, cleared in xylene, and coverslipped with Permount (Thermo Fisher Scientific). Images from stained sections were collected with a Leica fluorescent microscope equipped with an F-View II camera.

Detection of Dopamine Release with Dopamine Research ELISA Kit—Dopamine (DA) levels were determined using a dopamine research ELISA kit (Labor Diagnostika Nord, Nordhorn, Germany) according to the manufacturer's instructions. To determine the amount of DA released from differentiated cells with or without *Nurr1* and *Foxa2* transduction, N2 + ascorbic acid medium, conditioned in cells for 48 h, was collected.

DA release evoked by depolarization was also observed in differentiated cells. Cells at terminal differentiation on day 15 were incubated in N2 + ascorbic acid with (evoked) or without (basal release) 56 mM KCl for 30 min, and the medium was collected. Collected medium was stabilized with 4 mM sodium metabisulfite containing 1 mM EDTA, and DA levels were calculated using a standard curve obtained by plotting the absorbance readings based on standards (linear, y axis) against the corresponding standard concentrations (logarithmic, x axis).

Microarray—Total RNA was extracted with TRIzol (Invitrogen) and purified using RNeasy columns (Qiagen, Hilden, Germany) according to the manufacturer's instructions. Gene expression was measured using a MouseWG-6 BeadChip kit (Illumina, San Diego, CA). Raw data were imported into Illumina GenomeStudio software, and intensities were normalized using the cubic spline method. We selected only genes that exhibited significant levels of detection ($p < 0.01$) and a -fold change of ≥2 compared with day 0 at one or more time points after initiation of direct conversion.

Hierarchical clustering analysis was performed using log ratio-transformed expression data of selected genes with the complete linkage method and correlation distance, which was estimated from the cluster algorithm. The clustering result was visualized using TreeView (15).

Cell Counting and Statistical Analyses—Cell counting was performed with uniform random selection of 5–10 microscopic fields/well and 3–4 wells/experimental condition. All values were confirmed in at least three independent experiments. Data are expressed as the means ± S.E. A paired t test was performed when more than two groups were compared. Analyses were performed with SigmaPlot for Windows, version 10.0 (Systat Software GmbH, Erkrath, Germany).

Results

BAM-transduced Fibroblast Can Be Converted into NPCs—Previous studies have shown that fibroblasts transduced with a combination of neurogenic factors, including BAM, are directly converted into terminally differentiated neuronal cells. However, it remains to be determined whether fibroblast-to-neuron conversion is attained without passing through an intermediary stage for NPCs. To address this question, we isolated fibroblasts from transgenic mouse embryos expressing GFP under promoter control by nestin, an intermediate filament specific for NPCs (pNestin-GFP). Fibroblasts were cultured using the BAM-based trans-conversion protocol schematized in Fig. 1*A*. A fibroblast phenotype was confirmed by the expression of collagen I (COL1) and smooth muscle actin (SMA) (Fig. 1, *Bi* and *Bii*). None of the *in vitro* pNestin-GFP fibroblasts at day *in vitro* (DIV) 0 were positive for GFP (Fig. 1*B*), nestin, or SOX2 (Fig. 1, *Biii* and *Biv*), indicating that there was no neural tissue contamination during fibroblast preparation.

After growing in culture for 1–2 weeks, the BAM-transduced fibroblasts were transformed into small (cell body size: 10–20 μm) and slender cells with fine fiber outgrowths (usually bipolar; Fig. 1, *C* and *D*), which are characteristic features of neural lineage cells. Interestingly, GFP^+ cells (3.24 ± 2.42% of the total number of cells at DIV 10 (Fig. 1, *C* and *E*) appeared along with cells expressing the neuron-specific class III β-tubulin (TUJ1) in a mutually exclusive manner (Fig. 1*Di*). The percentage of GFP^+ cells increased to 13.12 ± 7.69% at DIV 20 (Fig. 1, *D* and *E*). In addition, nestin and SOX2 were co-localized in GFP-expressing cells (Fig. 1, *Dii* and *Diii*), confirming the NPC identity of the GFP^+ cells. Together, these findings suggested that

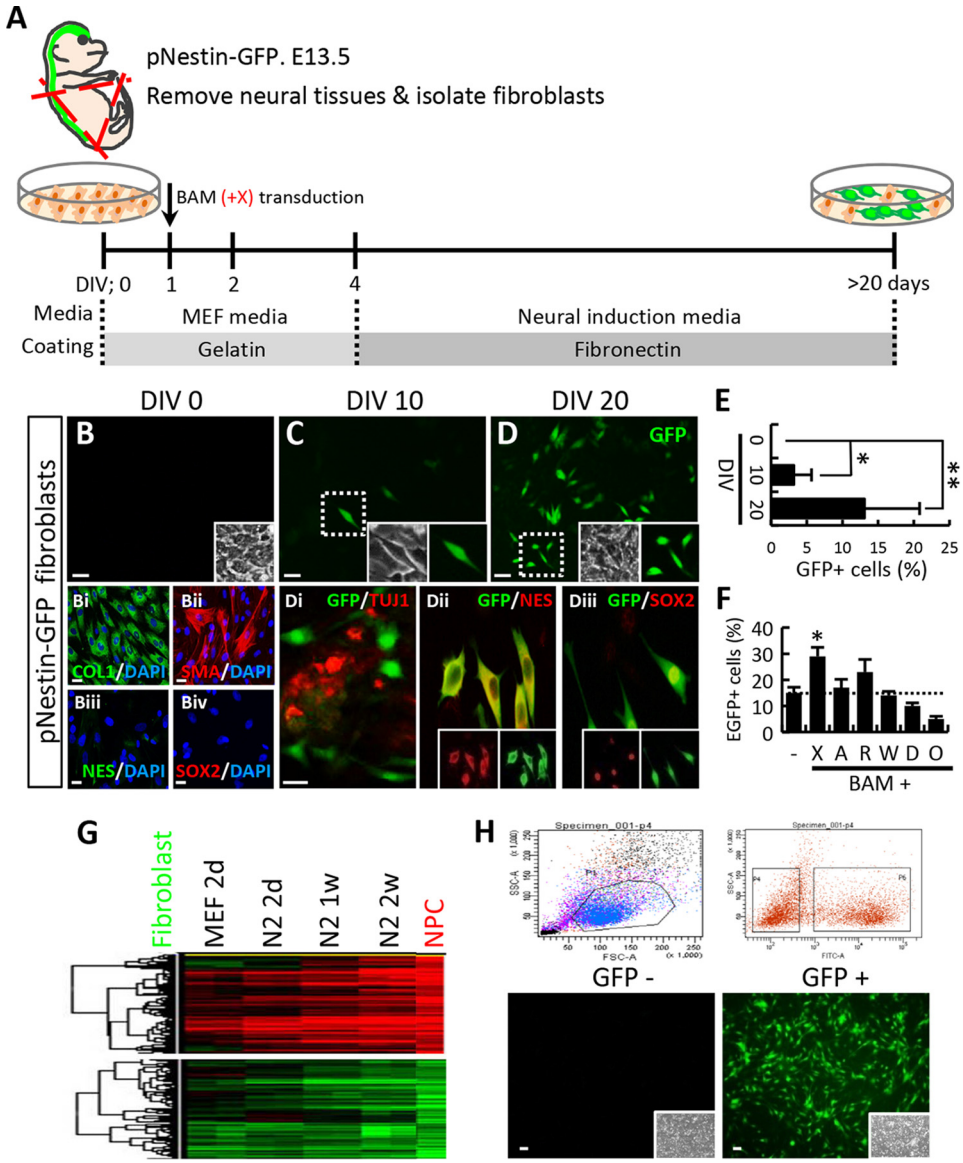

FIGURE 1. **Generation of iNPCs from mouse fibroblasts.** *A*, schematic diagram depicting the timeline of the iNPC conversion process. pNestin-GFP MEFs were transduced with BAM with and without other genes and monitored for GFP expression during proliferation. *B* and *Bi–Biv*, fibroblasts express collagen I (*COL1*, *Bi*) and SMA (*Bii*) but not the NPC markers, nestin (*NES*, *Biii*), or SOX2 (*Biv*). *C* and *E*, 6 days after neural induction (DIV 10), GFP^+ cells were observed. *D* and *E*, GFP^+ cells increased at DIV 20 (*insets* in *C* and *D* show representative higher magnification views). *Di–Diii*, although GFP^+ cells appeared along with $TUJ1^+$ neurons in a mutually exclusive pattern (*Di*), GFP^+ cells co-localized with the NPC markers nestin (*Dii*) and SOX2 (*Diii*). *F*, *Bcl-xL* (*X*), CA-*Akt* (*A*), CA-*Raf* (*R*), *Wnt1* (*W*), *Dlx2* (*D*), and *Otx2* (*O*) were co-transduced with BAM. *Bcl-xL* has a striking effect on GFP^+ cell yield. *G*, microarray data demonstrating the global gene expression pattern of the iNPC conversion period. *H*, FACS-based sorting against GFP expression. *Error bars*, S.E. *, $p < 0.05$; **, $p < 0.001$ compared with non-transduced fibroblasts (*E*) and compared with BAM-transduced cells (*F*). *Scale bar*, 20 μm.

BAM-transduced fibroblasts gave rise to not only neurons but also NPCs, and thus BAM transduction can be used as a strategy for fibroblast-to-NPC conversion.

Bcl-xL Contributes to iNPC Generation—To improve the NPC conversion efficiency, we tested co-expression of BAM with several other factors associated with NPC survival, proliferation, fate, and identity. Among the various factors tested, *Bcl-xL*, which is expressed in NPCs during brain development and is associated with survival and neuronal differentiation of NPCs (12, 16–19), exerted a significant improvement in GFP^+ cell yield (Fig. 1*F*).

Microarray analysis showed that the global gene expression pattern of fibroblasts transduced with BAM + *Bcl-xL* (BAMX) gradually transformed into one similar to that of NPCs derived from a mouse embryonic cortex after 2 weeks in culture (Fig. 1*G*). To obtain a uniform population of NPCs (hereafter referred to as "iNPCs"), we performed FACS-based sorting using GFP expression on BAMX-transduced pNestin-GFP cells at DIV 20. After sorting, the GFP^+ iNPC population reached >95% of total cells (Fig. 1*H*).

Bcl-xL has been reported to exert its anti-apoptotic effects through dimerization and mitochondrial localization. The percentage of $nestin^+$ or $SOX2^+$ cells in BAM-transduced cultures was similarly enhanced by co-expression of the *Bcl-xL* mutants in which the site for dimerization (Y101K) or mitochondrial localization (R209X) is abolished (Fig. 2*A*), with slightly lower efficiency than that of *Bcl-xL* wild type (Fig. 2, *B–D*). However, in our close examination, nestin and SOX2 immunoreactivities

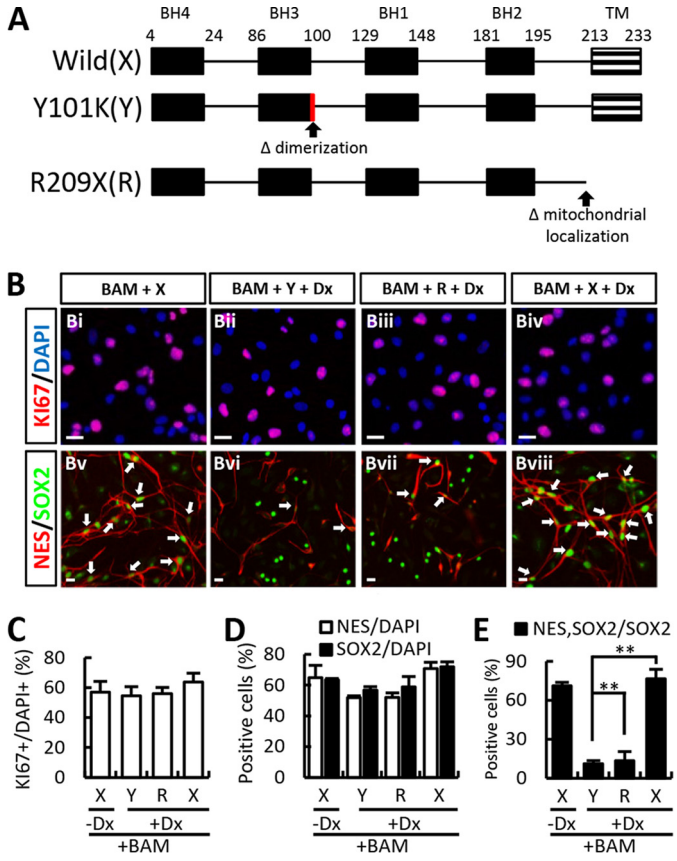

FIGURE 2. **The effect of *Bcl-xL* on iNPC yield is due not only to its anti-apoptotic functions but is also probably associated with its role in neural fate determination.** *A*, schematic representation of the different mutants tested: wild type *Bcl-xL* (*X*), Y101K (*Y*; dimerization-abolished mutant), and R209X (*R*; mitochondria localization-abolished mutant). *B–D*, BAMX-mediated trans-conversion was further improved in the presence of doxycycline (*Dx*). And BAM-mediated iNPC yield was similarly enhanced by co-expression of the Bcl-xL mutants with slightly lower efficiency than that of wild-type. *E*, co-expression of nestin and SOX2 was much lower in the cultures co-transduced with the *Bcl-xL* mutants than that of the wild-type (*arrows* indicate the co-localized of nestin and SOX2, *Bv–Bviii*). *Error bars*, S.E. **, $p < 0.001$ compared with wild-type *Bcl-xL* and supplemented Dx culture condition. *Scale bar*, 20 μm.

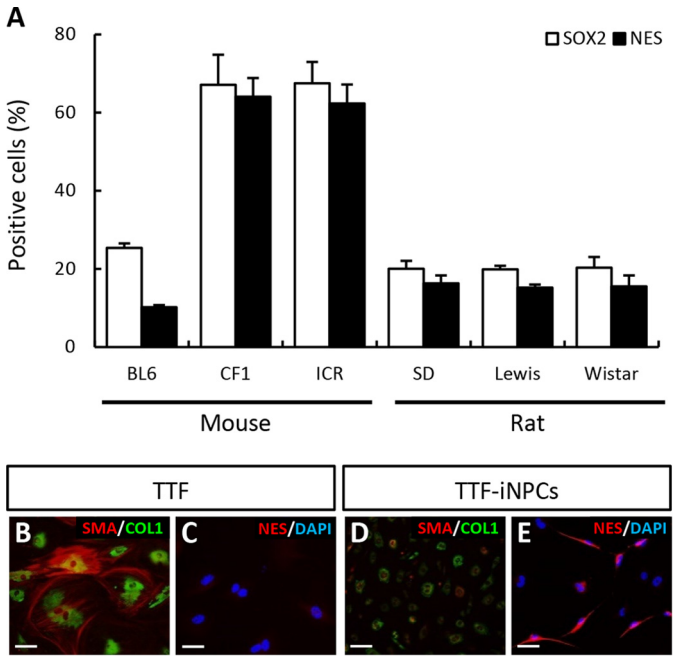

FIGURE 3. **Diverse iNPC conversion efficiency among species, strains, and adult mouse fibroblasts.** *A*, conversion efficiencies from three mouse strains (C57/BL6, CF1, and ICR) were slightly different. C57/BL6-derived fibroblast conversion efficiency was lower than CF1- and ICR-derived fibroblasts confirmed by nestin$^+$ or SOX2$^+$ cell number. In the case of rat fibroblasts, there were no differences among strains. Conversion efficiency of rat fibroblasts was lower than that of mouse strains (CF1 and ICR); however, the nestin$^+$ and SOX2$^+$ cell percentages were calculated from total cells, including cluster and non-cluster cells. After counting only purified cluster cells, nestin$^+$ and SOX2$^+$ cell percentages increased significantly. *B–E*, loss of fibroblast identity and gain of NPC-related gene expression in TTF-iNPCs. The representative markers collagen I (*COL1*; *B* and *D*, *green*) and SMA (*B* and *D*, *red*) of fibroblasts were decreased in iNPCs. Conversely, iNPCs expressed the NPC marker for nestin (*E*, *red*) compared with TTF (*C*). Unfortunately, the conversion efficiency was lower than embryonic fibroblasts. *Scale bar*, 20 μm.

were not well co-localized in the mutant-expressing cultures, and thus the percentage of cells co-expressing nestin and SOX2 was much lower in the cultures cotransduced with the *Bcl-xL* mutants than that of the wild type; the percentages of nestin$^+$SOX2$^+$ cells of total SOX2$^+$ cells were as follows: 76.53 ± 7.28% (BAM + *Bcl-xL* wild type), 11.14 ± 2.28% (BAM + *Bcl-xL* Y101K mutant), and 13.46 ± 7.01% (BAM + *Bcl-xL* R209X mutant) (Fig. 2, *B* and *E*). These findings suggest that anti-apoptotic action and/or actions of *Bcl-xL* mediated by the dimerization and mitochondrial co-localization contribute at least in part to facilitating BAM-induced iNPC generation.

We and others recently reported that Dx exerts a protective effect in pluripotent cells and neural cells at various stages of development (20–22). Consistent with these effects of Dx on survival, Dx supplementation afforded healthier cultures during the trans-differentiation procedure (data not shown). Likewise, the BAMX-mediated trans-conversion was further improved in the presence of Dx (percentage of nestin$^+$ cells in the absence *versus* presence of Dx: 64.82 ± 7.97% *versus* 70.72 ± 4.08%, respectively; percentage of SOX2$^+$ cells: 63.40 ± 0.86% *versus* 71.97 ± 3.06%, respectively; $n = 3$ culture dishes; Fig. 2, *B–D*). Based on these findings, all subsequent experiments were performed using Dx-supplemented medium unless otherwise indicated.

iNPC Conversion Efficiency from Embryonic Fibroblasts Derived from Different Strains, Species, and Adult Mouse Fibroblasts—BAMX-mediated trans-conversion of fibroblasts derived from different species and strains was estimated according to the number of cells that exhibited immunoreactivity to NPC markers at DIV 21 (Fig. 3*A*). The trans-conversion efficiency from the fibroblasts prepared from C57/BL6 mice, which is the background strain of pNestin-GFP transgenic mice, was comparable with that of the transgenic animals (nestin$^+$ and SOX2$^+$ cells at DIV 21: 10.20 ± 0.55 and 25.36 ± 1.15%). Likewise, the number of nestin$^+$SOX2$^+$ cells converted from ICR- and CF1-derived fibroblasts was greater than for C57/BL6-derived fibroblasts. Last, BAMX-induced trans-conversion was efficiently induced from fibroblasts derived from each of the three different rat embryos tested regardless of strain.

We detected nestin$^+$ NPCs in cultures of the fibroblasts derived from adult mouse tail tip (TTF) 4 weeks after BAMX transduction (Fig. 3, *C* and *E*), along with loss of the fibroblast-specific markers COL1 and SMA (Fig. 3, *B* and *D*), indicating that the BAMX-mediated strategy also worked for adult fibro-

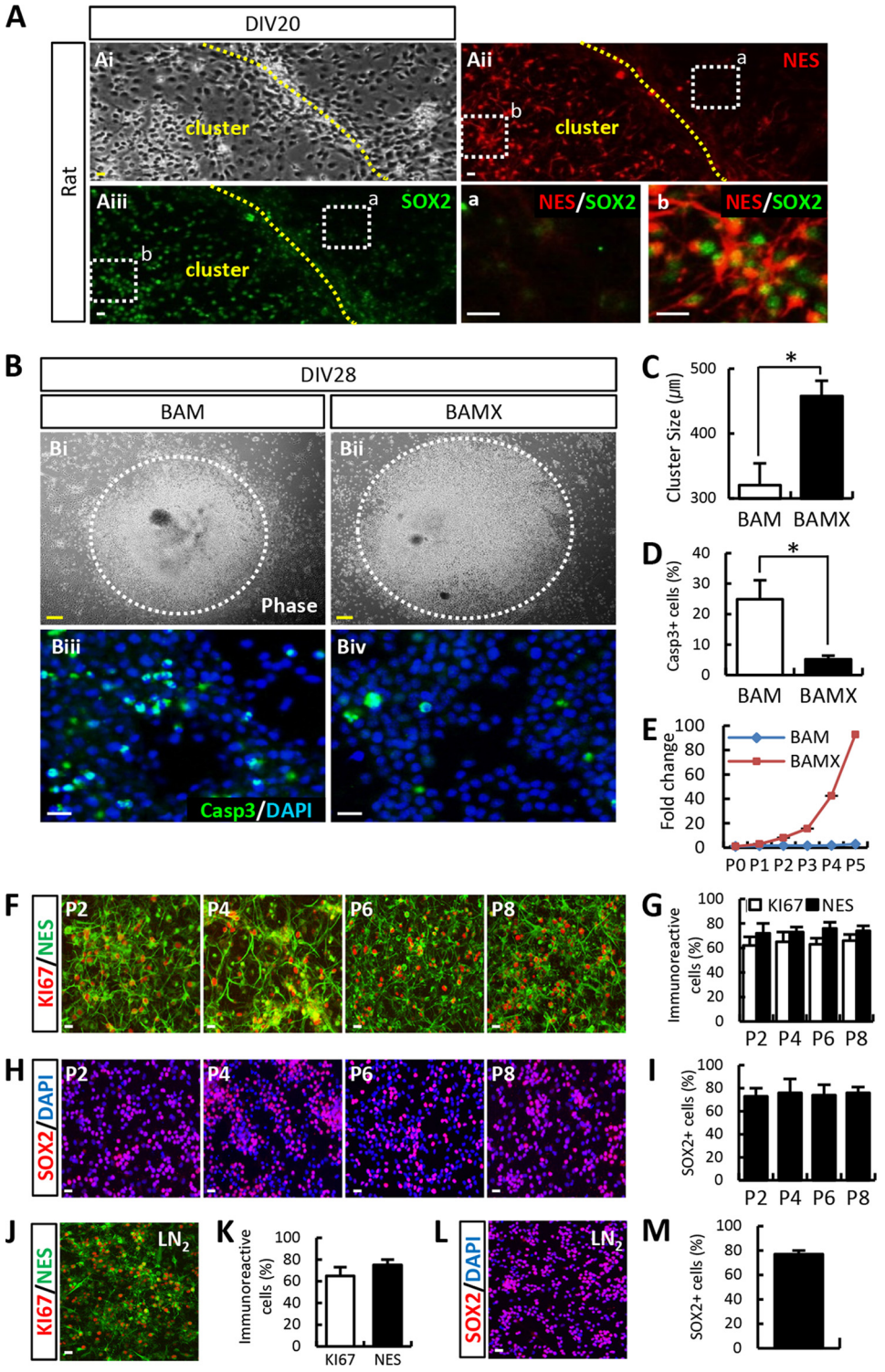

FIGURE 4. **BAMX-derived iNPCs are highly expandable while maintaining their NPC properties.** *A* and *Ai–Aiii*, during conversion under culture conditions, the cells exhibited a cluster morphology with a bipolar appearance (*Ai*). Cluster-forming cells expressed nestin (*Aii*) and SOX2 (*Aiii*), whereas non-cluster cells expressed neither nestin nor SOX2 (*a*, nestin$^-$/SOX2$^-$ cells in non-cluster cells; *b*, nestin$^+$/SOX2$^+$ cells in cluster cells; *a* and *b* represent *higher magnification views* of *Aii* and *Aiii*). *B–E*, iNPCs are efficiently induced and proliferate following expression of *Bcl-xL*. Although neural precursor-like cells (cluster form) were observed under BAM-transduced conditions, the cluster size was smaller, and these cells did not proliferate (*Bi*, *C*, and *E*), unlike BAMX-transduced cells (*Bii*, *C*, and *E*). The number of iNPCs increased more than 90-fold compared with the first stage (*E*), and the number of cleaved caspase-3 (*casp3*)$^+$ cells decreased following BAMX transduction (*Biii–Biv* and *D*). *F–I*, iNPCs were stably expandable without loss of self-renewing potential. *J–M*, after freezing and thawing at passage 22, iNPCs do not lose their self-renewal potential. Notably, no significant change was observed in the expression of NPC markers KI67/nestin (*J* and *K*) and SOX2$^+$ after freezing and thawing (*L* and *M*, respectively). *Error bars*, S.E. *, $p < 0.05$, compared with BAM-transduced cells. *Scale bar*, 20 μm (Fig. 2, *Bi* and *Bii*; *scale bar*, 100 μm).

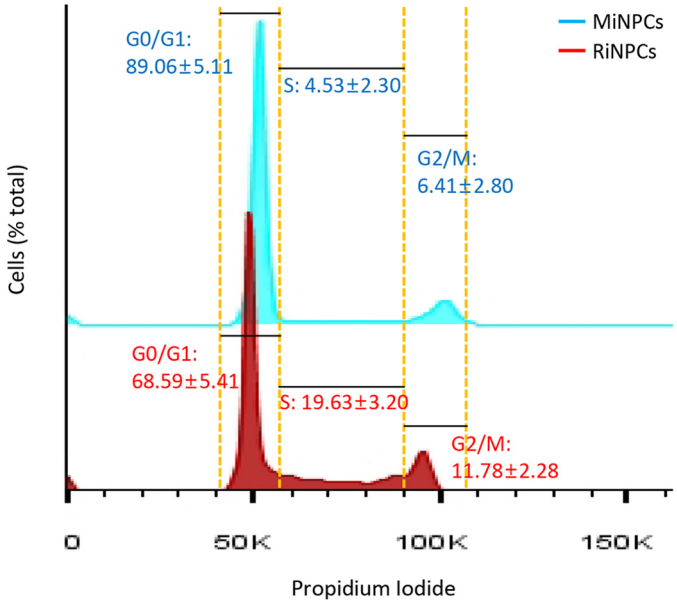

FIGURE 5. **Cell proliferation properties are different between rat and mouse fibroblast-derived iNPCs.** Rat and mouse fibroblasts were transduced with BAMX. iNPCs were isolated when neural precursor-like cell morphology was observed. Rat and mouse fibroblasts were induced to iNPCs in N2 medium containing bFGF, FGF8, LIF, and doxycycline (*Dx*) or bFGF, EGF, FGF8, LIF, and doxycycline, respectively. Cell cycle properties were analyzed by FACS. Interestingly, rat-derived iNPCs (*RiNPCs*, *red*) had higher proliferative properties compared with mouse-derived iNPCs (*MiNPCs*, *blue*), as evidenced by relative S phase cell abundance. The S phase percentages are 19.63 ± 3.20% *versus* 4.53 ± 2.30% for rat and mouse iNPCs, respectively (*, $p < 0.05$).

blasts. However, consistent with previous reports (23), the transconversion efficiency was quite low (nestin$^+$ cells: <1%).

iNPCs Derived from BAMX-transduced Rat Fibroblasts Are Highly Expandable and Maintain Their NPC Properties—Cell expansion is a requirement for iNPCs to be a stable experimental and transplantable cell source. However, for reasons that are not yet understood, we observed species-dependent differences in cell proliferation. Among the iNPCs derived from all the mouse fibroblasts tested, *in vitro* expansion was not induced, even in the presence of various NPC-specific mitogens, such as bFGF, epidermal growth factor (EGF), sonic hedgehog (SHH), FGF8, LIF, Dx (20), and any combination thereof, although cell numbers decreased slightly due to apoptosis (data not shown). In contrast, iNPCs derived from rat fibroblasts were readily induced to proliferate with the bFGF + FGF8 + LIF + Dx mitogen combination, forming proliferating cell clusters that expressed the NPC markers nestin and SOX2 (Fig. 4*A*). Additionally, the results of FACS-based analysis were consistent with our observation of species-dependent differences in cell proliferation with respect to the percentage of cells in the S phase of iNPC cultures (rat, 19.63 ± 3.20% *versus* mouse, 4.53 ± 2.30%) (Fig. 5).

Because nestin$^+$SOX2$^+$ cells accumulated in clusters of cultured rat cells (Fig. 4*A*), we harvested iNPC clusters using mechanical scraping followed by dissociation into single cells and subculturing the cells with various mitogens. Cell expansion, as estimated by cluster size (Fig. 4, *Bi*, *Bii*, and *C*), was greater in the presence of *Bcl-xL* expression and was associated with a marked reduction in cell apoptosis (Fig. 4, *Biii*, *Biv*, and *D*). Furthermore, iNPCs that were derived through BAM transduction underwent massive cell apoptosis during consecutive passaging procedures, resulting in a decrease in cell number (Fig. 4*E*). A lack of cell expandability in BAM-derived rat iNPCs was observed in multiple experiments with various combinations of NPC-specific mitogens. In contrast, iNPCs derived from BAMX fibroblasts were highly and continuously expanded over multiple passages without altering NPC-specific nestin and SOX2 expression (Fig. 4, *F–I*). Indeed, BAMX-transduced rat iNPCs could be expanded for 110 cell passages (5–7 days/passage) with a 2–5-fold cell number increase after every passage. Rat iNPCs could be stored in liquid N_2 and recultured with a high cell viability (>70% cell survival after thawing) and without requiring nestin$^+$/SOX2$^+$ expression for cell population change (Fig. 4, *J–M*). Given the feasibility of rat iNPCs as a stable cell source, further experiments were performed using BAMX-induced rat iNPCs unless otherwise indicated.

Regional Identity and Differentiation of Rat iNPCs—Expression of glia fibrillary acidic protein (GFAP), brain lipid-binding protein, and radial glia cell marker-2 (RC2), all of which are expressed in NPCs of adult brains and radial glial cells, were not co-localized in our iNPCs (data not shown), implying that the iNPCs generated in this study may be more similar to prototypical embryonic (fetal) NPCs rather than those of adult brain origin. Nevertheless, high expression of the general NPC markers (nestin, SOX2, and PAX6) in the rat iNPCs and regional markers specific for embryonic forebrain, midbrain, hindbrain, and spinal cord were only slightly expressed compared with NPC cultures derived from the respective embryonic brain tissues, indicating that the regional identity of iNPCs was undetermined (Fig. 6*A*).

When terminal differentiation of the iNPCs (at passage 2; P2) was induced by mitogen withdrawal, the cells differentiated toward TUJ1$^+$ neurons (5–10% of the total DAPI$^+$ cells; Fig. 6*Bi*) and GFAP$^+$ astrocytes (50–60%; Fig. 5*Bii*). On the other hand, few if any oligodendrocytes were detected in the differentiated cultures (Fig. 6*Biii*). The propensity for astrogenic differentiation is a property of NPCs that is derived from the brain during middle/late gestation. Expression of markers specific for general excitatory (glutamate; Fig. 6*Biv*) and inhibitory (GABA; Fig. 6*Bv*) neurons was weakly localized in the TUJ1$^+$ neuronal cells derived from iNPCs. In addition, none of the TUJ1$^+$ cells in the differentiated cultures expressed markers for dopaminergic (TH; Fig. 6*Bvi*), serotonergic (serotonin; Fig. 6*Bvii*), or cholinergic (choline acetyltransferase; data not shown) neurons, which specifically arise from the embryonic midbrain, hindbrain, and spinal cord, respectively. In addition to low or undetectable region-specific marker expressions in the iNPCs (Fig. 6*A*), these findings were consistent with our observation that regional identity and neuronal subtype differentiation potential were not specified in the iNPCs.

Manipulation of iNPC Differentiation toward Neurons and Midbrain-type Dopamine Neurons—Treatment of extrinsic factors known to facilitate neurogenesis, including brain-derived neurotrophic factor, neurotropin-3, and glial cell line-derived neurotrophic factor, did not enhance neuronal yields from the iNPCs (data not shown). However, neuron yield increased markedly after transduction of pro-neural bHLH genes neurogenin 2 (*Ngn2*; Fig. 6, *Ci*, *Cii*, and *D*) and *Mash1*

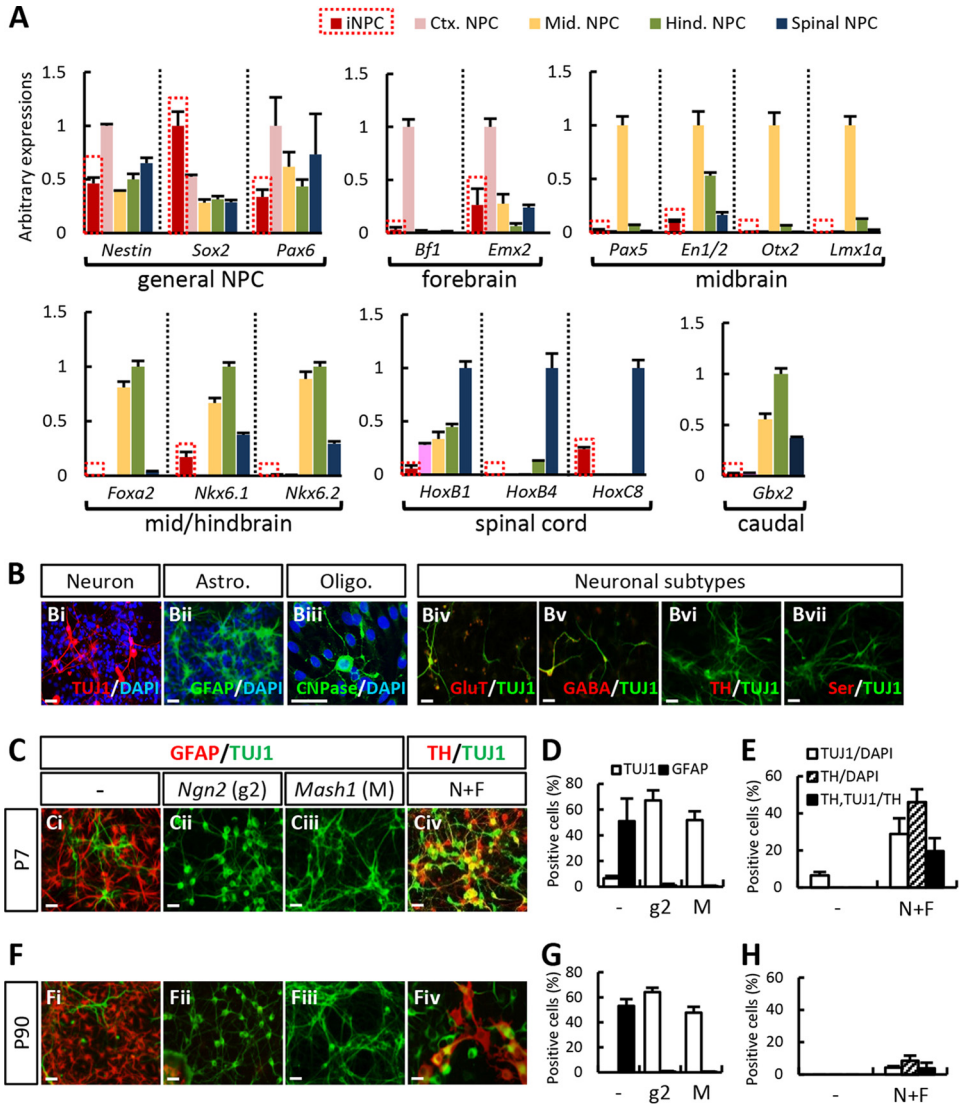

FIGURE 6. **iNPCs have unidentified regional identity.** *A*, general NPC and embryonic region-related expression markers as determined by quantitative real-time PCR. Rat iNPCs expressed general NPC markers; however, regional specific markers were expressed only slightly compared with NPC cultures derived from respective embryonic brain tissues. *B*, iNPCs have the potential to differentiate into one of three cell types: neurons (*Bi*), astrocytes (*Bii*), and oligodendrocytes (*Biii*). Markers specific for general excitatory (glutamate (*GluT*), *Biv*) and inhibitory (GABA, *Bv*) neurons were weakly localized in the TUJ1$^+$ neuronal cells derived from iNPCs. However, markers specific for dopaminergic (TH, *Bvi*) and serotonergic (serotonin (*ser*), *Bvii*) activity were not expressed. *C–E*, early iNPCs (P7) exhibited a highly astrogenic differentiation potential (Ci). The neuronal yield was markedly increased by transduction of pro-neural bHLH genes, neurogenin 2 (*Ngn2*, *Cii* and *D*), or *Mash1* (*Ciii* and *D*), whereas GFAP$^+$ cells were markedly reduced (*D*). Also, N+F-transduced iNPC-derived dopamine neurons expressed TH and produced an increased number of TUJ1$^+$ cells (*Civ* and *E*). *F–H*, in long term passaged iNPCs (P90), the number of TUJ1$^+$ cells decreased, whereas GFAP$^+$ cell numbers remained stable (*Fi* and *G*). The effects of *Ngn2* or *Mash1* transduction were similar to that of early passaged iNPCs (P7, *Fii*, *Fiii*, and *G*); however, the TH$^+$ cell yield was far lower than that of P7 cultures. In particular, TH$^+$ cells exhibited an immature morphology (*Fiv* and *H*). *Error bars*, S.E. *Scale bar*, 30 μm.

(*Ascl1*; Fig. 6, *Ci*, *Ciii*, and *D*), along with a robust reduction of astrocyte numbers (percentage of TUJ1$^+$ neurons *versus* percentage of GFAP$^+$ astrocytes of total cells (TUJ1/GFAP) at P7 = 6.47 ± 1.84%/50.97 ± 17.60% (control), 67.15 ± 7.89%/0.91 ± 1.25% (*Ngn2*-transduced), and 51.77 ± 6.78%/0.36 ± 0.32% (*Mash1*-transduced cultures)). Together, these findings indicated that the astrogenic differentiation properties of iNPCs were not fixed and could be readily manipulated toward a specific neuronal fate by expression of the appropriate neurogenic genes.

Our study aimed to derive midbrain-type DA (mDA) neurons from iNPCs and to use these cells as a therapeutic approach for PD. Previous studies have shown that the combined expression of *Nurr1* and *Foxa2* (N+F) in cultured NPCs that were sufficiently derived from a rodent brain drives mDA neuron differentiation by inducing the acquisition of an mDA phenotype as well as neuronal differentiation. Consistently, DA neurons co-expressing the DA neuron-specific marker TH and neuron-specific marker TUJ1 were abundantly yielded from iNPCs at P7 by N+F transduction (Fig. 6, *Civ* and *E*).

Ngn2 and *Mash1* transduction in late passaged iNPCs (P90) also greatly enhanced TUJ1$^+$ neuronal yields at the expense of GFAP$^+$ astrocyte yields (Fig. 6, *Fi–Fiii* and *G*). Meanwhile, the changes in TUJ1$^+$/GFAP$^+$ cell numbers were comparable with those from early passaged iNPCs (P7). However, combined N+F expression in P90 cultures resulted in somewhat different

outcomes from those of P7 cultures. Specifically, TUJ1$^+$ and TH$^+$ cell yields in P90 cultures increased in response to N+F transduction, but the extent of this increase was far lower than that of P7 cultures. Furthermore, TH$^+$ cells did not exhibit a neuron-like morphology, and the expression for the TUJ1 neuron marker was localized in only a few TH$^+$ cells. The percentage of TH$^+$TUJ1$^+$ cells relative to the total TH+ cell population was 19.63 ± 6.97% at P7 *versus* 3.88 ± 3.42% at P90 (Fig. 6, *Fiv* and *H*). Due to a lack of neuronal differentiation in the TH$^+$ cells yielded from late passaged iNPCs, the experiments

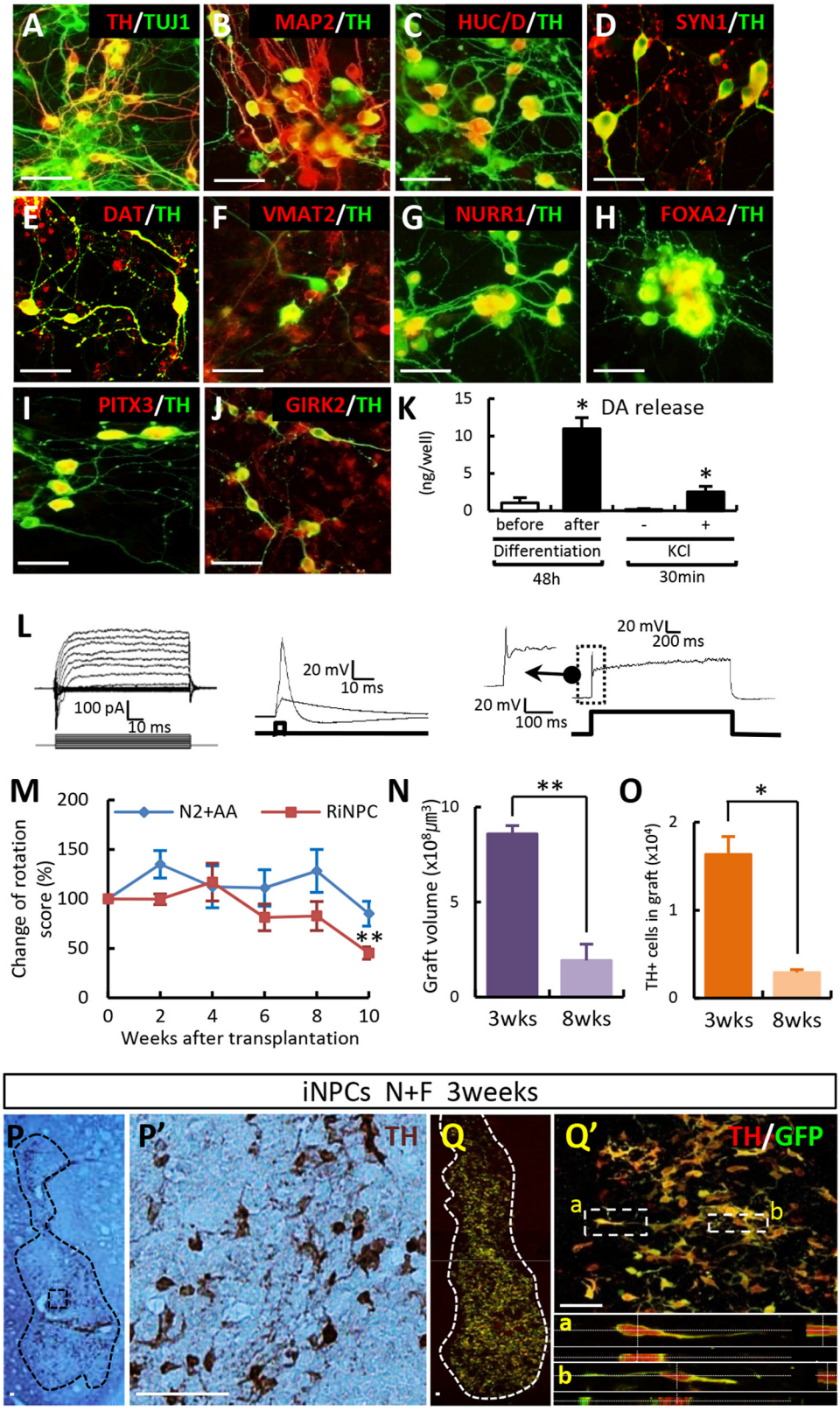

described below were performed using iNPCs at an early stage of passage (up to P10).

Functionality of iNPC-derived DA neurons in Vitro and in Vivo after Transplantation—We next examined TH^+ DA cells yielded from N+F-transduced iNPCs. TH^+ cells differentiated from N+F-transduced iNPCs (P7) appeared as morphologically mature neurons with multiple and extensive neurite outgrowths and expressed all of the neuron-specific markers for which we tested, including TUJ1, microtubule-associated protein 2 (MAP2), HuC/D, and synapsin I (Fig. 7, *A–D*). Dopamine transporter (DAT) and vesicular monoamine transporter 2 (VMAT2), proteins involved in DA homeostasis were co-localized in TH^+ neurons (Fig. 7, *E* and *F*). In addition to exogenously expressed *Nurr1* and *Foxa2* (Fig. 7, *G* and *H*), iNPC-derived TH^+ DA neuronal cells expressed proteins specific for mDA neuron (PITX3) and A9-type (nigral) mDA neuron (potassium inwardly rectifying channel subfamily J, member 6; GIRK2) (Fig. 7, *I* and *J*). Whole-cell patch clamp analysis showed that the neuronal cells that differentiated from N+F-transduced iNPCs produced sodium and potassium currents and were capable of firing action potentials (Fig. 7*L*).

DA (10.98 ± 1.48 ng/well, $n = 3$) was readily detected in the medium of N+F-transduced iNPC cultures 15 days after differentiation. Furthermore, DA release was instigated by a 56 mM KCl-induced depolarization stimulus (2.52 ± 0.76 ng/30 min/well, $n = 3$; Fig. 7*K*). These findings collectively indicated that we successfully derived midbrain-type DA neurons that were mature morphologically, phenotypically, and functionally and that appeared to be competent as presynaptic DA neurons *in vitro*. Combinatory N+F + *Ngn2* expression was also effective with respect to generating mature/functional DA neurons from iNPCs derived from mouse fibroblasts (Fig. 8).

Our final set of experiments examined the *in vivo* functionality of iNPC-derived mDA neurons by transplantation into PD model rats. An amphetamine-induced rotation test showed that rats grafted with N+F-transduced iNPCs exhibited a significant reduction in their rotation scores compared with sham-control animals (percentage of pretransplantation scores at 10 weeks after transplantation = 45.3 ± 6.25% ($n = 8$) *versus* 85.1 ± 12.48% ($n = 6$); **, $p < 0.001$; Fig. 7*M*). N+F-iNPC transplantation generated grafts (volume = 8.58 ± 1.92 mm^3; Fig. 7*N*) 3 weeks post-transplantation that contained 16,373 ± 2,010 TH^+ cells (Fig. 7*O*). However, unlike the *in vitro* setting, TH^+ cells in the graft did not exhibit a fully mature neuronal morphology. Instead, the cells exhibited short bipolar or unipolar fiber outgrowths (Fig. 7, *P* and *Q*). Histologic assessment performed 8 weeks after transplantation revealed a severe reduction in graft volume (0.44 ± 0.86 mm^3; Fig. 7*N*) and TH^+ cell number (2,932 ± 298 cells; Fig. 7*O*).

Taken together, these findings suggest a critical difference in the maturity and function of DA neurons derived from iNPCs *in vivo* in transplanted brains and those from *in vitro* cultures. Indeed, neuronal differentiation/maturation and survival of DA neurons after iNPC transplantation remain critical issues that will require further investigation.

Discussion

Wernig *et al.* (6) showed that BAM-transduced fibroblasts are directly converted to postmitotic neuronal cells without an intermediary NPC stage. Although it is possible that NPCs were present in their study, they could not be detected, probably because they quickly disappeared after being generated due to further differentiation into neurons or apoptosis. We addressed this problem in our study using fibroblasts derived from pNestin-GFP mouse embryos and showed that at least a portion of BAM-transduced fibroblasts were converted into NPCs. A major difference in the experimental conditions of our study compared with those from the study by Vierbuchen *et al.* (6) was our exogene expression system. Specifically, we used a retroviral vector system, whereas Vierbuchen *et al.* (6) used a lentiviral system. Thus, the level and maintenance of exogenous BAM expression, which can affect trans-conversion efficiency and speed, was expected to be different during the trans-conversion period. Notably, exogene expression in retroviral systems, but not lentiviral systems, is frequently silenced, especially during neuron differentiation and among different types of neuronal cells (24–27). Thus, it is likely that the BAM proteins induced by the retroviral vector in our study were active during the trans-differentiation procedure throughout the NPC stages but were later silenced during terminal NPC differentiation toward a neuron fate. Without exogenous BAM expression, terminal differentiation of NPCs was blocked, and NPCs were detected in abundance.

Fibroblast-to-iNPC conversion in recent studies has been attained via gradual silencing of exogene expression using retroviral vector systems (10, 28, 29). Consistently, we also observed a substantial loss of BAMX expression during terminal differentiation of NPCs. According to real-time PCR analysis, mRNA levels of *Brn2*, *Ascl1*, *Myt1L*, and *Bcl-xL* relative to those before differentiation were only 0.15, 0.16, 0.43, and 0.06 after 7 days of differentiation, respectively. By contrast, Vierbuchen lentivirus-transduced cells probably retained stable BAM expression without silencing, which may have more efficiently driven NPC differentiation toward a postmitotic neuron fate. In the terminal differentiation condition, which is the most efficient, NPCs rapidly differentiate as soon as they are generated from BAM fibroblasts and cannot be easily detected.

FIGURE 7. **Functional midbrain-like DA neurons are induced from iNPCs *in vitro* and can be transplanted into a PD rat model.** *A–D*, N+F-transduced iNPCs differentiated over a 10–15-day period. TH^+ cells co-expressed neuron-specific markers (TUJ1, MAP2, HuC/D, and synapsin I (SYN1)). *E* and *F*, DA homeostasis markers DAT and VMAT2. *G* and *H*, exogenously expressed NURR1 and FOXA2. *I*, TH^+ cells expressed proteins specific for mDA neurons (PITX3). *J*, A9 type midbrain marker GIRK2 co-localized with TH^+ cells. *K* and *L*, presynaptic DA neuronal functions as seen on electrophysiological analysis (*L*) and DA release assay (*K*). DA release was evoked by high potassium-induced depolarization stimulus in differentiated cells. *M–Q*, *in vivo* behavior (*M–O*) and histological analyses (*P* and *Q*) after transplantation. Behavioral recovery was assessed by amphetamine-induced rotation in sham-operated animals (N2 + ascorbic acid (*AA*), $n = 6$) and NF-induced DA cells (*RiNPC*, $n = 8$) (*M*). Graphs depict the graft volume (*N*) and total number of TH^+ cells in grafts between 3 and 8 weeks post-transplantation (*O*). At 3 weeks post-transplantation, the presence of GFP-labeled donor iNPCs co-expressed TH^+ cells (*P*, DAB; *Q*, immunofluorescence image). *P′*, higher magnification views of *P*; *Q′*, region adjacent to *Q*; *a* and *b*, higher magnification views of *Q′*). *Error bars*, S.E. *, $p < 0.05$, compared with the control (*K*). *, $p < 0.05$; **, $p < 0.001$ compared with week 0 (*M*) and 3 weeks after transplantation (*N* and *O*). *Scale bar*, 50 μm.

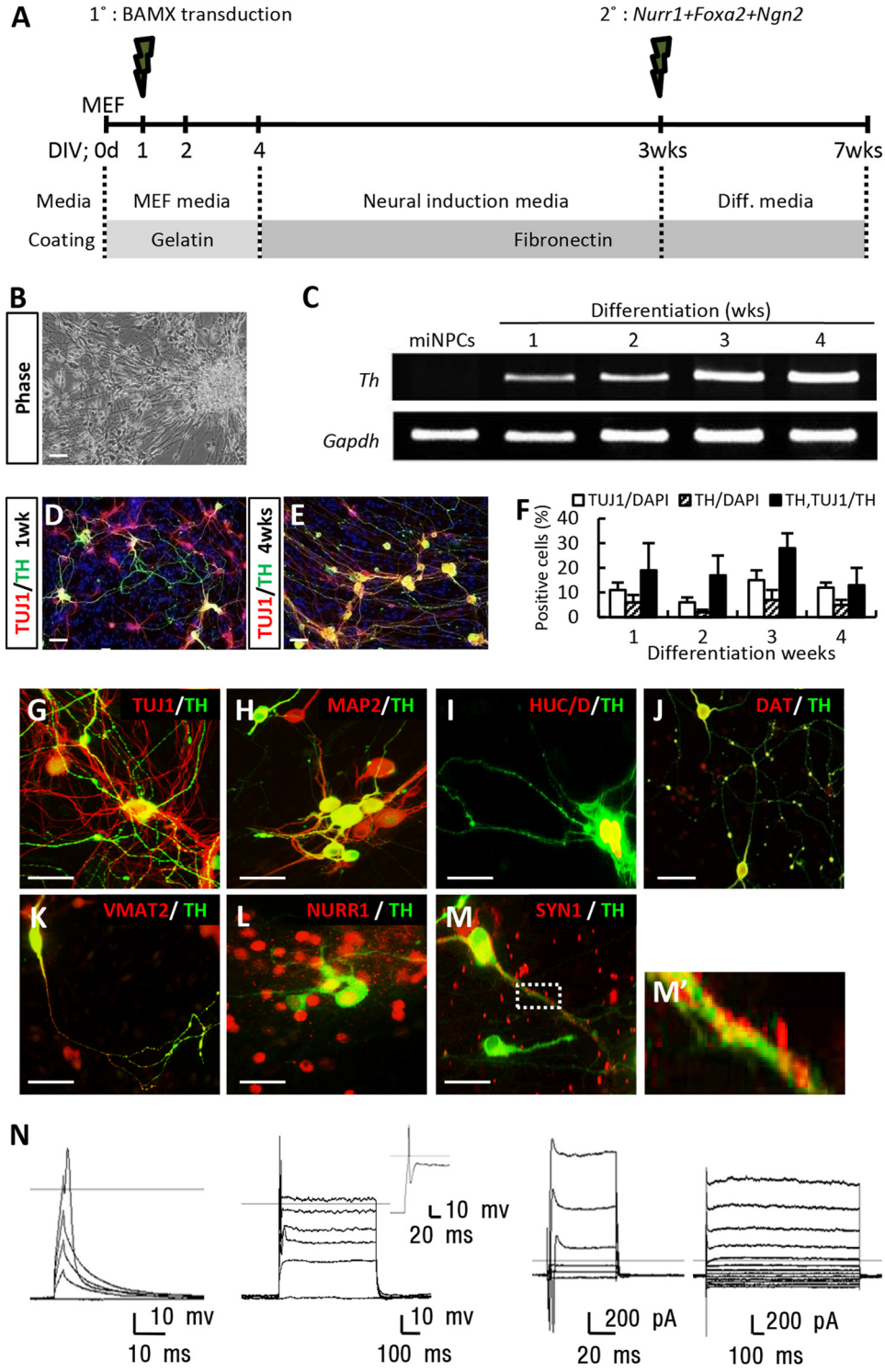

FIGURE 8. **CF1 mouse fibroblast-derived iNPCs can be generated from functional mDA neurons *in vitro*.** *A*, schematic diagram depicting the timeline of the MiNPC conversion process. *B*, phase-contrast image of differentiated MiNPC morphology. *C–F*, TH^+TUJ1^+ cells were generated during DA differentiation conditions in *Nurr1* + *FoxA2* + neurogenin 2-transduced MiNPCs. Similar to REF-iNPCs, MEF-iNPCs generated functional DA neurons. After differentiation for 10 days, TH^+ cells co-expressed neuron-specific markers (TUJ1, MAP2, and HuC/D) (*G–I*), DA homeostasis markers (DAT and VMAT2) (*J* and *K*), marker specific for midbrain (NURR1) (*L*), and synapse formation marker (synapsin I; *SYN1*) (*M*). *M'*, higher magnification view of *M*; *N*, electrophysiological analysis. *Error bars*, S.E. *Scale bars*, 20 μm (*B–E*) and 50 μm (*G–M*).

A major benefit of reprogramming toward NPCs instead of neurons is the ability to utilize cell proliferation to provide a scalable source for neurons and other neural cell types. However, iNPCs derived from BAM fibroblasts underwent replicative cell senescence during the early proliferation phase for unidentified reasons. Here, we showed that co-expression of the anti-apoptotic factor *Bcl-xL* along with BAM (BAMX) led to iNPCs that were highly proliferative over a long period of time and grew over 100 passages without alterations in major NPC properties.

Numerous roles of *Bcl-xL* in NPC survival and maintenance have been documented previously in knock-out mouse embryonic brains (16), *in vitro* with gain-of-function studies using NPC cultures (30, 31), and in clonal analyses using mouse embryonic neural precursor cells transduced with *Bcl-xL* (data not shown). To investigate whether the observed effects of *Bcl-xL* were due to its pro-survival functions, we analyzed the effect of *Bcl-xL* on the conversion of fibroblasts to iNPCs using dimerization- and mitochondrial localization-deficient *Bcl-xL* mutants (18). Importantly, cells expressing the mutant *Bcl-xL* constructs were able to generate iNPCs. Thus, the role of *Bcl-xL* in iNPC generation may be due to both its neurogenic functions and pro-survival effects.

In the last 3 years, several methods for fibroblast-to-NPC conversion have been described that use curtailed versions of four-iPSC factor-based reprogramming (10, 32) or new gene expression combinations. With the exception of NSC-specific gene expression and their self-renewal properties, diverse methods generate iNPCs with a variety of differentiation phenotypes and regional identities.

Although expression of a few genes specific for certain brain regions was found in our iNPCs, none were fully consistent with any specific regional identity. Moreover, none of the region-specific genes that we tested were highly expressed in BAMX-induced iNPCs, indicating their ambiguous regional identity. Thus, methods for reprogramming toward certain region-specific NPCs remain to be developed. Similar to previous studies (7, 10, 33), our iNPCs preferentially differentiated into astrocytes. Considering that BAM are neurogenic genes, preferential astrocytic differentiation is unexpected. For the iNPCs in our study, the unusual astrocytic differentiation may have been due to silencing of exogene expression. On the other hand, the differentiation propensity was not fixed and could be readily manipulated into neuronal differentiation by additional neurogenic gene expression.

Practical use of iNPCs in therapies and in research makes subtype neuronal differentiations from iNPCs important because specific neuronal subtypes may be affected by neurologic disorders. Importantly, we were able to achieve efficient generation of midbrain-type DA neurons from iNPCs in PD-affected models. The mDA neurons derived from iNPCs were fully mature in their morphology and phenotype *in vitro*, and avid presynaptic DA neuron functions were observed. However, when the iNPCs were transplanted into the striatum of PD rats, the engrafted DA neurons were relatively immature with short and mostly bipolar neurite outgrowths, and survival of these cells long after transplantation was not ensured. The difference between *in vitro* and *in vivo* neuronal maturity makes sense, considering that the *in vivo* environment of a transplanted brain cannot be expected to support NPC differentiation and survival. Rather, we expect this environment to be hostile, consisting of inflammatory and immune responses that are in stark contrast to the *in vitro* culture conditions that afforded enriched trophic support for these cells. Development of further intrinsic programming in donor NPCs is required to design a method wherein these cells can efficiently survive and differentiate while overcoming a hostile host environment after transplantation.

Similar to our study, previous studies addressed the *in vivo* functionality of DA neurons directly converted from fibroblasts in transplanted PD rats (34, 35). Among these studies, the behavioral recovery and DA neuron yield in the study by Kim *et al.* are comparable with our findings. However, neither study was able to suggest a satisfactory level of DA neuron engraftment and functionality from transplantation. Further research is needed to establish an appropriate trans-differentiation strategy for cell-therapeutic approaches.

References

1. Campbell, K. H., McWhir, J., Ritchie, W. A., and Wilmut, I. (1996) Sheep cloned by nuclear transfer from a cultured cell line. *Nature* **380,** 64–66
2. Gurdon, J. B., Elsdale, T. R., and Fischberg, M. (1958) Sexually mature individuals of *Xenopus laevis* from the transplantation of single somatic nuclei. *Nature* **182,** 64–65
3. Cowan, C. A., Atienza, J., Melton, D. A., and Eggan, K. (2005) Nuclear reprogramming of somatic cells after fusion with human embryonic stem cells. *Science* **309,** 1369–1373
4. Tada, M., Takahama, Y., Abe, K., Nakatsuji, N., and Tada, T. (2001) Nuclear reprogramming of somatic cells by *in vitro* hybridization with ES cells. *Curr. Biol.* **11,** 1553–1558
5. Takahashi, K., and Yamanaka, S. (2006) Induction of pluripotent stem cells from mouse embryonic and adult fibroblast cultures by defined factors. *Cell* **126,** 663–676
6. Vierbuchen, T., Ostermeier, A., Pang, Z. P., Kokubu, Y., Südhof, T. C., and Wernig, M. (2010) Direct conversion of fibroblasts to functional neurons by defined factors. *Nature* **463,** 1035–1041
7. Lujan, E., Chanda, S., Ahlenius, H., Südhof, T. C., and Wernig, M. (2012) Direct conversion of mouse fibroblasts to self-renewing, tripotent neural precursor cells. *Proc. Natl. Acad. Sci. U.S.A.* **109,** 2527–2532
8. Lujan, E., and Wernig, M. (2012) The many roads to Rome: induction of neural precursor cells from fibroblasts. *Curr. Opin. Genet. Dev.* **22,** 517–522
9. Maucksch, C., Jones, K. S., and Connor, B. (2013) Concise review: the involvement of SOX2 in direct reprogramming of induced neural stem/precursor cells. *Stem Cells Transl. Med.* **2,** 579–583
10. Thier, M., Wörsdörfer, P., Lakes, Y. B., Gorris, R., Herms, S., Opitz, T., Seiferling, D., Quandel, T., Hoffmann, P., Nöthen, M. M., Brüstle, O., and Edenhofer, F. (2012) Direct conversion of fibroblasts into stably expandable neural stem cells. *Cell Stem Cell* **10,** 473–479
11. Kim, S. M., Flasskamp, H., Hermann, A., Araúzo-Bravo, M. J., Lee, S. C., Lee, S. H., Seo, E. H., Lee, S. H., Storch, A., Lee, H. T., Schöler, H. R., Tapia, N., and Han, D. W. (2014) Direct conversion of mouse fibroblasts into induced neural stem cells. *Nat. Protoc.* **9,** 871–881
12. Chang, M. Y., Sun, W., Ochiai, W., Nakashima, K., Kim, S. Y., Park, C. H., Kang, J. S., Shim, J. W., Jo, A. Y., Kang, C. S., Lee, Y. S., Kim, J. S., and Lee, S. H. (2007) Bcl-XL/Bax proteins direct the fate of embryonic cortical precursor cells. *Mol. Cell. Biol.* **27,** 4293–4305
13. Park, C. H., Kang, J. S., Yoon, E. H., Shim, J. W., Suh-Kim, H., and Lee, S. H. (2008) Proneural bHLH neurogenin 2 differentially regulates Nurr1-induced dopamine neuron differentiation in rat and mouse neural precursor cells *in vitro*. *FEBS Lett.* **582,** 537–542
14. He, X. B., Yi, S. H., Rhee, Y. H., Kim, H., Han, Y. M., Lee, S. H., Lee, H., Park, C. H., Lee, Y. S., Richardson, E., Kim, B. W., and Lee, S. H. (2011) Prolonged membrane depolarization enhances midbrain dopamine neuron differentiation via epigenetic histone modifications. *Stem Cells* **29,** 1861–1873
15. Eisen, M. B., Spellman, P. T., Brown, P. O., and Botstein, D. (1998) Cluster analysis and display of genome-wide expression patterns. *Proc. Natl. Acad. Sci. U.S.A.* **95,** 14863–14868
16. Motoyama, N., Wang, F., Roth, K. A., Sawa, H., Nakayama, K., Nakayama, K., Negishi, I., Senju, S., Zhang, Q., and Fujii, S. (1995) Massive cell death of immature hematopoietic cells and neurons in Bcl-x-deficient mice. *Science* **267,** 1506–1510
17. Shim, J. W., Koh, H. C., Chang, M. Y., Roh, E., Choi, C. Y., Oh, Y. J., Son, H.,

Lee, Y. S., Studer, L., and Lee, S. H. (2004) Enhanced *in vitro* midbrain dopamine neuron differentiation, dopaminergic function, neurite outgrowth, and 1-methyl-4-phenylpyridium resistance in mouse embryonic stem cells overexpressing Bcl-XL. *J. Neurosci.* **24,** 843–852

18. Park, C. H., Kang, J. S., Shin, Y. H., Chang, M. Y., Chung, S., Koh, H. C., Zhu, M. H., Oh, S. B., Lee, Y. S., Panagiotakos, G., Tabar, V., Studer, L., and Lee, S. H. (2006) Acquisition of in vitro and in vivo functionality of Nurr1-induced dopamine neurons. *FASEB J.* **20,** 2553–2555
19. Gross, A., McDonnell, J. M., and Korsmeyer, S. J. (1999) BCL-2 family members and the mitochondria in apoptosis. *Genes Dev.* **13,** 1899–1911
20. Chang, M. Y., Rhee, Y. H., Yi, S. H., Lee, S. J., Kim, R. K., Kim, H., Park, C. H., and Lee, S. H. (2014) Doxycycline enhances survival and self-renewal of human pluripotent stem cells. *Stem Cell Rep.* **3,** 353–364
21. Yrjänheikki, J., Keinänen, R., Pellikka, M., Hökfelt, T., and Koistinaho, J. (1998) Tetracyclines inhibit microglial activation and are neuroprotective in global brain ischemia. *Proc. Natl. Acad. Sci. U.S.A.* **95,** 15769–15774
22. Jantzie, L. L., Cheung, P. Y., and Todd, K. G. (2005) Doxycycline reduces cleaved caspase-3 and microglial activation in an animal model of neonatal hypoxia-ischemia. *J. Cereb. Blood Flow Metab.* **25,** 314–324
23. Esteban, M. A., Wang, T., Qin, B., Yang, J., Qin, D., Cai, J., Li, W., Weng, Z., Chen, J., Ni, S., Chen, K., Li, Y., Liu, X., Xu, J., Zhang, S., Li, F., He, W., Labuda, K., Song, Y., Peterbauer, A., Wolbank, S., Redl, H., Zhong, M., Cai, D., Zeng, L., and Pei, D. (2010) Vitamin C enhances the generation of mouse and human induced pluripotent stem cells. *Cell Stem Cell* **6,** 71–79
24. Hamaguchi, I., Woods, N. B., Panagopoulos, I., Andersson, E., Mikkola, H., Fahlman, C., Zufferey, R., Carlsson, L., Trono, D., and Karlsson, S. (2000) Lentivirus vector gene expression during ES cell-derived hematopoietic development *in vitro*. *J. Virol.* **74,** 10778–10784
25. Laker, C., Meyer, J., Schopen, A., Friel, J., Heberlein, C., Ostertag, W., and Stocking, C. (1998) Host cis-mediated extinction of a retrovirus permissive for expression in embryonal stem cells during differentiation. *J. Virol.* **72,** 339–348
26. Rhee, Y. H., Ko, J. Y., Chang, M. Y., Yi, S. H., Kim, D., Kim, C. H., Shim, J. W., Jo, A. Y., Kim, B. W., Lee, H., Lee, S. H., Suh, W., Park, C. H., Koh, H. C., Lee, Y. S., Lanza, R., Kim, K. S., and Lee, S. H. (2011) Protein-based human iPS cells efficiently generate functional dopamine neurons and can treat a rat model of Parkinson disease. *J. Clin. Invest.* **121,** 2326–2335
27. Vroemen, M., Weidner, N., and Blesch, A. (2005) Loss of gene expression in lentivirus- and retrovirus-transduced neural progenitor cells is correlated to migration and differentiation in the adult spinal cord. *Exp. Neurol.* **195,** 127–139
28. Han, D. W., Tapia, N., Hermann, A., Hemmer, K., Höing, S., Araúzo-Bravo, M. J., Zaehres, H., Wu, G., Frank, S., Moritz, S., Greber, B., Yang, J. H., Lee, H. T., Schwamborn, J. C., Storch, A., and Schöler, H. R. (2012) Direct reprogramming of fibroblasts into neural stem cells by defined factors. *Cell Stem Cell* **10,** 465–472
29. Ring, K. L., Tong, L. M., Balestra, M. E., Javier, R., Andrews-Zwilling, Y., Li, G., Walker, D., Zhang, W. R., Kreitzer, A. C., and Huang, Y. (2012) Direct reprogramming of mouse and human fibroblasts into multipotent neural stem cells with a single factor. *Cell Stem Cell* **11,** 100–109
30. Lee, H. S., Bae, E. J., Yi, S. H., Shim, J. W., Jo, A. Y., Kang, J. S., Yoon, E. H., Rhee, Y. H., Park, C. H., Koh, H. C., Kim, H. J., Choi, H. S., Han, J. W., Lee, Y. S., Kim, J., Li, J. Y., Brundin, P., and Lee, S. H. (2010) Foxa2 and Nurr1 synergistically yield A9 nigral dopamine neurons exhibiting improved differentiation, function, and cell survival. *Stem Cells* **28,** 501–512
31. Akamatsu, W., DeVeale, B., Okano, H., Cooney, A. J., and van der Kooy, D. (2009) Suppression of Oct4 by germ cell nuclear factor restricts pluripotency and promotes neural stem cell development in the early neural lineage. *J. Neurosci.* **29,** 2113–2124
32. Kim, J., Efe, J. A., Zhu, S., Talantova, M., Yuan, X., Wang, S., Lipton, S. A., Zhang, K., and Ding, S. (2011) Direct reprogramming of mouse fibroblasts to neural progenitors. *Proc. Natl. Acad. Sci. U.S.A.* **108,** 7838–7843
33. Matsui, T., Takano, M., Yoshida, K., Ono, S., Fujisaki, C., Matsuzaki, Y., Toyama, Y., Nakamura, M., Okano, H., and Akamatsu, W. (2012) Neural stem cells directly differentiated from partially reprogrammed fibroblasts rapidly acquire gliogenic competency. *Stem Cells* **30,** 1109–1119
34. Kim, J., Su, S. C., Wang, H., Cheng, A. W., Cassady, J. P., Lodato, M. A., Lengner, C. J., Chung, C. Y., Dawlaty, M. M., Tsai, L. H., and Jaenisch, R. (2011) Functional integration of dopaminergic neurons directly converted from mouse fibroblasts. *Cell Stem Cell* **9,** 413–419
35. Liu, X., Li, F., Stubblefield, E. A., Blanchard, B., Richards, T. L., Larson, G. A., He, Y., Huang, Q., Tan, A. C., Zhang, D., Benke, T. A., Sladek, J. R., Zahniser, N. R., and Li, C. Y. (2012) Direct reprogramming of human fibroblasts into dopaminergic neuron-like cells. *Cell Res.* **22,** 321–332